

---

# Multifaceted Quadruplet of Low-Lying Spin-Zero States in $^{66}\text{Ni}$ : Emergence of Shape Isomerism in Light Nuclei

S. Leoni,<sup>1,2,\*</sup> B. Fornal,<sup>3</sup> N. Mărginean,<sup>4</sup> M. Sferrazza,<sup>5</sup> Y. Tsunoda,<sup>6</sup> T. Otsuka,<sup>6,7,8,9</sup> G. Bocchi,<sup>1,2</sup> F. C. L. Crespi,<sup>1,2</sup>  
A. Bracco,<sup>1,2</sup> S. Aydin,<sup>10</sup> M. Boromiza,<sup>4,11</sup> D. Bucurescu,<sup>4</sup> N. Cieplicka-Oryńczak,<sup>2,3</sup> C. Costache,<sup>4</sup> S. Călinescu,<sup>4</sup>  
N. Florea,<sup>4</sup> D. G. Ghiță,<sup>4</sup> T. Glodariu,<sup>4</sup> A. Ionescu,<sup>4,11</sup> Ł.W. Iskra,<sup>3</sup> M. Krzysiek,<sup>3</sup> R. Mărginean,<sup>4</sup> C. Mihai,<sup>4</sup> R. E. Mihai,<sup>4</sup>  
A. Mitu,<sup>4</sup> A. Negreț,<sup>4</sup> C. R. Niță,<sup>4</sup> A. Olăcel,<sup>4</sup> A. Oprea,<sup>4</sup> S. Pascu,<sup>4</sup> P. Petkov,<sup>4</sup> C. Petrone,<sup>4</sup> G. Porzio,<sup>1,2</sup> A. Șerban,<sup>4,11</sup>  
C. Sotty,<sup>4</sup> L. Stan,<sup>4</sup> I. Știru,<sup>4</sup> L. Stroe,<sup>4</sup> R. Șuvăilă,<sup>4</sup> S. Toma,<sup>4</sup> A. Turturică,<sup>4</sup> S. Ujenuc,<sup>4</sup> and C. A. Ur<sup>12</sup>

<sup>1</sup>*Dipartimento di Fisica, Università degli Studi di Milano, I-20133 Milano, Italy*

<sup>2</sup>*INFN sezione di Milano via Celoria 16, 20133, Milano, Italy*

<sup>3</sup>*Institute of Nuclear Physics, PAN, 31-342 Kraków, Poland*

<sup>4</sup>*Horia Hulubei National Institute of Physics and Nuclear Engineering—IFIN HH, Bucharest 077125, Romania*

<sup>5</sup>*Département de Physique, Université libre de Bruxelles, B-1050 Bruxelles, Belgium*

<sup>6</sup>*Center for Nuclear Study, University of Tokyo, Hongo, Bunkyo-ku, Tokyo 113-0033, Japan*

<sup>7</sup>*Department of Physics, University of Tokyo, Hongo, Bunkyo-ku, Tokyo 113-0033, Japan*

<sup>8</sup>*National Superconducting Cyclotron Laboratory, Michigan State University, East Lansing, Michigan 48824, USA*

<sup>9</sup>*Instituut voor Kern- en Stralingsfysica, KU Leuven, B-3001 Leuven, Belgium*

<sup>10</sup>*Department of Physics, University of Aksaray, Adana E-90 Karayolu Üzeri, Aksaray, Turkey*

<sup>11</sup>*University of Bucharest, Faculty of Physics, Bucharest-Magurele, 077125, Romania*

<sup>12</sup>*Extreme Light Infrastructure—Nuclear Physics, IFIN-HH, Bucharest, 077125, Romania*

A search for shape isomers in the  $^{66}\text{Ni}$  nucleus was performed, following old suggestions of various mean-field models and recent ones, based on state-of-the-art Monte Carlo shell model (MCSM), all considering  $^{66}\text{Ni}$  as the lightest nuclear system with shape isomerism. By employing the two-neutron transfer reaction induced by an  $^{18}\text{O}$  beam on a  $^{64}\text{Ni}$  target, at the sub-Coulomb barrier energy of 39 MeV, all three lowest-excited  $0^+$  states in  $^{66}\text{Ni}$  were populated and their  $\gamma$  decay was observed by  $\gamma$ -coincidence technique. The  $0^+$  states lifetimes were assessed with the plunger method, yielding for the  $0_2^+$ ,  $0_3^+$ , and  $0_4^+$  decay to the  $2_1^+$  state the  $B(E2)$  values of 4.3, 0.1, and 0.2 Weisskopf units (W.u.), respectively. MCSM calculations correctly predict the existence of all three excited  $0^+$  states, pointing to the oblate, spherical, and prolate nature of the consecutive excitations. In addition, they account for the hindrance of the  $E2$  decay from the prolate  $0_4^+$  to the spherical  $2_1^+$  state, although overestimating its value. This result makes  $^{66}\text{Ni}$  a unique nuclear system, apart from  $^{236,238}\text{U}$ , in which a retarded  $\gamma$  transition from a  $0^+$  deformed state to a spherical configuration is observed, resembling a shape-isomerlike behavior.

The concept of potential energy surface (PES) is central in many areas of physics. Usually, the PES displays the potential energy of the system as a function of its geometry. As an example, the PES of a molecule expressed in such coordinates as bond length, valence angles, etc., can be used for finding the minimum energy shape or calculating chemical reaction rates [1]. The idea of potential energy surface in deformation space has also been widely applied to the nucleus at a given spin. For an even-even nucleus at spin 0, the lowest PES minimum corresponds to the ground state (g.s.), while there may exist additional (secondary) minima in which excited  $0^+$  states can reside: they can be interpreted as ground states of different shapes [2–6]. When a secondary minimum is separated from the main minimum by a high barrier, in the extreme case a long-lived isomer, called *shape isomer*, can be formed [7]. Shape isomerism at spin zero, so far, has clearly been observed only in actinide nuclei - these isomers decay mainly by fission, and in

two cases only,  $^{236}\text{U}$  and  $^{238}\text{U}$ , by very retarded  $\gamma$ -ray branches [8–11].

The existence of shape isomers in lighter systems has been a matter of debate for a long time. Already in the 1980s, a study based on microscopic Hartree-Fock plus BCS calculations, in which a large number of nuclei was surveyed, identified ten isotopes in which a deformed  $0^+$  state is separated from a spherical structure by a significantly high barrier:  $^{66}\text{Ni}$  and  $^{68}\text{Ni}$ ,  $^{190,192}\text{Pt}$ ,  $^{206,208,210}\text{Os}$ , and  $^{194,196,214}\text{Hg}$  [12]. Other investigations [13,14], which used a nonaxial Hartree-Fock-Bogoliubov approach, selected a rather restricted number of candidates, among which the lightest were  $^{66,68}\text{Ni}$ ,  $^{74,76}\text{Kr}$ ,  $^{78,80,98}\text{Sr}$ ,  $^{80,82,100}\text{Zr}$ , and  $^{86}\text{Mo}$ . Quite recently, Möller *et al.* [15] presented a global study of potential energy surfaces in 7206 nuclei from  $A = 31$  to  $A = 290$  by employing a well-benchmarked macroscopic-microscopic finite-range

liquid-drop model [16]. Here, secondary PES minima at spin 0 were found in a few tens of nuclei, among which  $^{66}\text{Ni}$  was also present. To summarize,  $^{66}\text{Ni}$  is the lightest system for which all three models, discussed above, suggest the existence of a pronounced secondary PES minimum which may give rise to shape isomerism.

Recently, state-of-the-art shell model calculations became capable of calculating shape coexistence in nuclei with masses  $A = 60\text{--}100$  [17–22]. In particular, it became possible to assess transition probabilities between states of different shapes, and to search for retarded decays which would be the signature of a shape-isomerlike structure. Monte Carlo shell model (MCSM) studies [23–26] have been performed for the neutron-rich  $^{68\text{--}78}\text{Ni}$  isotopes and coexistence of low-lying spherical, oblate, and strongly deformed prolate shapes has been found in  $^{68}\text{Ni}$  and  $^{70}\text{Ni}$  [17,18]. A significant hindrance for the  $E2$  transition deexciting the prolate deformed  $0^+$  state was predicted in  $^{68}\text{Ni}$  only. On the experimental side, the lifetimes of the supposedly well-deformed prolate  $0^+$  states, located at 2511 and 1567 keV in  $^{68}\text{Ni}$  [27,28] and  $^{70}\text{Ni}$  [29,30], respectively, were assessed in a very recent  $\beta$ -decay study of  $^{68}\text{Co}$  and  $^{70}\text{Co}$  [31]. No hindrance was observed in both cases, pointing to a substantial mixing (or a low potential barrier) between deformed and spherical configurations in  $^{68}\text{Ni}$  and  $^{70}\text{Ni}$  isotopes.

At this point, we turned our attention to  $^{66}\text{Ni}$ , for which mean-field calculations already predicted a secondary PES deep minimum [12–16]. We performed new theoretical and experimental studies of  $^{66}\text{Ni}$  low-lying states, with a particular focus on  $0^+$  states. The theoretical investigation was carried out within the Monte Carlo shell model [23–26], using the same Hamiltonian and model space as the ones previously employed for  $^{68\text{--}78}\text{Ni}$  [17]. Figure 1 shows the potential energy surface of  $^{66}\text{Ni}$ , obtained similarly to Refs. [17,18,32]. In comparison with  $^{68}\text{Ni}$ , the barrier height is similar, but the prolate minimum is lower in  $^{66}\text{Ni}$ , due to stronger  $p - n$  interaction coming from more neutron holes in the  $N = 40$  closed shell. As a consequence, a more strict hindrance to the decay to the main spherical minimum, from the prolate one, is expected in  $^{66}\text{Ni}$ . The circles on the plot of Fig. 1 indicate the intrinsic quadrupole moments of a given basis vector of the MCSM eigenstate, and their size implies the overlap probability of this basis vector with the eigenwave function [17,18].

In Fig. 1, the circles are concentrated in spherical ( $0_1^+$  and  $0_3^+$ ), oblate ( $0_2^+$ ), and prolate ( $0_4^+$ ) domains, with  $\beta_2 \approx 0.0$ ,  $-0.2$ , and  $0.3$ , respectively. While the local minimum in the prolate domain is profound, due to a shell evolution of type II [18], the one in the oblate domain is very shallow, being almost a shoulder.

With respect to the  $0_1^+$  state, the  $0_{2,4}^+$  states are found to be composed of sizable excitations of protons, from  $f_{7/2}$  to  $f_{5/2}$  and  $p_{3/2,1/2}$ , as well as neutrons, from  $f_{5/2}$  and  $p_{3/2,1/2}$  to  $g_{9/2}$  and  $d_{5/2}$ . In the  $0_2^+$  state,  $\sim 1$  proton and  $\sim 1.5$

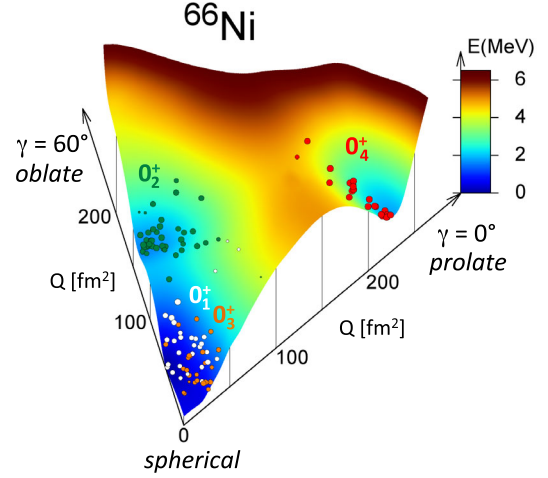


FIG. 1. Potential energy surface (PES) for the lowest  $0^+$  states of  $^{66}\text{Ni}$ , as a function of prolate and oblate quadrupole moments. Circles on the PES represent shapes in the MCSM basis vectors: white (orange) circles for  $0_1^+$  ( $0_3^+$ ) spherical states, green (red) for  $0_2^+$  oblate ( $0_4^+$  prolate) states, respectively.

neutrons are excited, whereas these numbers are doubled in the  $0_4^+$  state. This large difference in particle-hole excitations leads to very different deformations between  $0_2^+$  and  $0_4^+$  states. On the contrary, the  $0_{1,3}^+$  and  $2_1^+$  states have similar occupation numbers, being spherical.

The reduced probabilities for  $E2$  transitions deexciting the  $0_2^+$  oblate,  $0_3^+$  spherical, and  $0_4^+$  prolate states to the spherical  $2_1^+$  state are 4.1, 0.01, and 0.006 Weisskopf units (W.u.), respectively. While the retardation of the  $0_4^+$  decay arises from the prolate to spherical shape change, the hindrance of the spherical  $0_3^+$  decay is caused by cancellation effects in the  $E2$  transition matrix elements due to different structures within spherical states.

Experimentally, a first inspection of  $^{66}\text{Ni}$  data, established prior to our study, already shows remarkable features in line with the MCSM calculations: three excited  $0^+$  states (out of a total of 6 excitations below 3 MeV) have been located at 2444, 2664, and 2965 keV by using a  $(t,p)$  reaction [33]. Out of those, the first two were confirmed by the discrete  $\gamma$ -ray studies of [27,34,35] and their energies were determined with higher precision at 2443 and 2671 keV. On the contrary, the  $0_4^+$  state was not observed. We propose that these three  $0^+$  excited states correspond to the three  $0^+$  excitations predicted by the MCSM calculations at 1971 (oblate), 2596 (spherical), and 3296 keV (prolate), respectively [see Figs. 2(d) and (e)]. This experiment-theory correspondence is supported by two independent observations: (i) both experiment [27,35,36] and MCSM calculations show that, out of the four  $0^+$  states in  $^{66}\text{Ni}$ , the  $\beta$  decay of the  $1^+$  ground state of  $^{66}\text{Co}$  feeds only the spherical ground state and the  $0_3^+$  state, what points to similarly spherical (although configuration-wise different) structures of these two states; (ii) in the  $(t,p)$  reaction study [33], the population of the  $0_2^+$  and  $0_3^+$  states is strongly

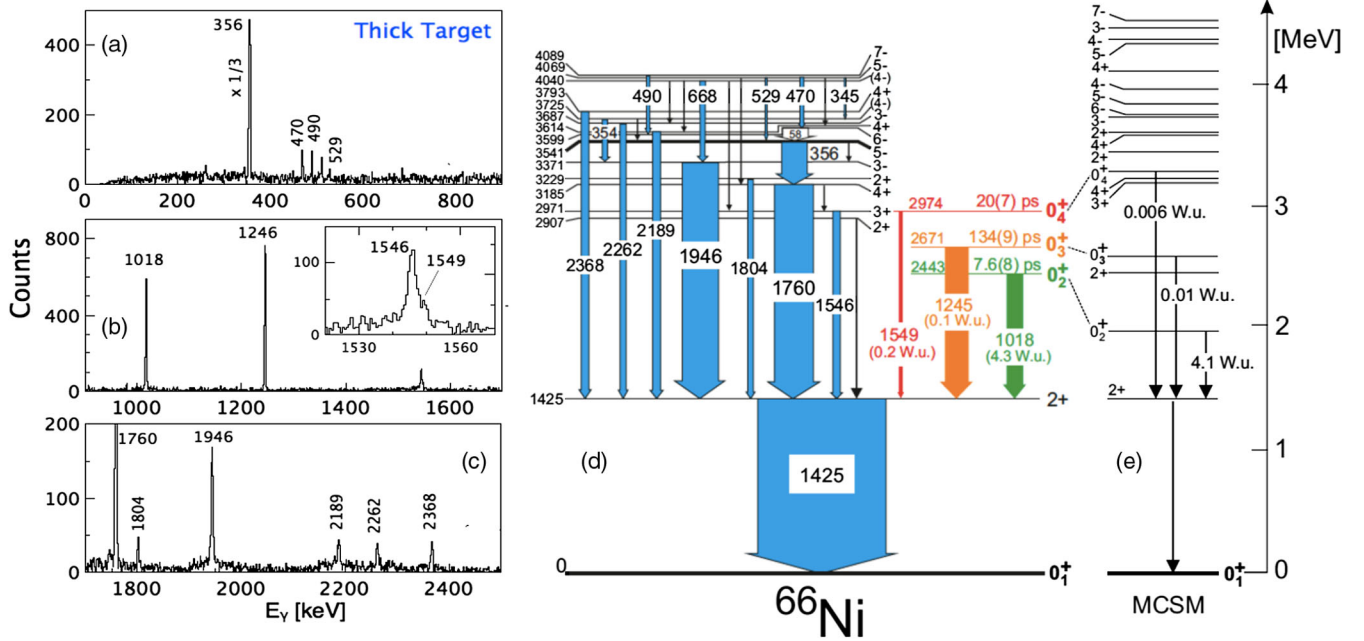


FIG. 2. (a)–(c)  $\gamma$ -ray spectrum of  $^{66}\text{Ni}$  gated by  $2_1^+ \rightarrow 0_1^+$  1425-keV transition, observed in the thick-target measurement. (d) Decay scheme of  $^{66}\text{Ni}$  observed in the experiment (black-thin arrows for known transitions [34] not seen here). (e) Results from MCSM calculations.

avored over the population of the  $0_4^+$  excitation (by a factor of 7 and 12, respectively).

To establish experimentally more detailed characteristics of the  $0^+$  excitations in  $^{66}\text{Ni}$ , we undertook a new experimental study of their lifetimes, at the Tandem Laboratory of the Horia Hulubei National Institute for Physics and Nuclear Engineering (IFIN-HH) in Bucharest. The states of interest were populated in a  $2n$ -transfer reaction induced by a beam of  $^{18}\text{O}$  on a  $^{64}\text{Ni}$  target, at incident energy (39 MeV) below the Coulomb barrier. The power of this approach resides in the fact that the fusion-evaporation channel, which is highly favored above the Coulomb barrier, is severely hindered in this case - its cross section becomes comparable to the one of the  $2n$ -transfer process (few mb).

The  $\gamma$  transitions of  $^{66}\text{Ni}$  were measured using the ROSPHERE array [37], consisting of 14 Ge detectors and 11  $\text{LaBr}_3(\text{Ce})$  scintillators. A first part of the experiment was carried out with a  $5 \text{ mg/cm}^2$  thick target of  $^{64}\text{Ni}$ . A total of about  $10^8$   $\gamma$ - $\gamma$  coincidences were collected in a 6 day-long run with a beam intensity of more than 30 pNA. Figures 2(a)–2(c) display a spectrum obtained by setting a gate on the  $2^+ \rightarrow 0^+$ , 1425 keV, ground state transition in  $^{66}\text{Ni}$ . All visible  $\gamma$  rays correspond to transitions previously located in  $^{66}\text{Ni}$  [34] and deexciting all known states below  $\approx 4.1$  MeV excitation energy [Fig. 2(d)].

In the spectrum of Figs. 2(a)–2(c), a number of transitions shows tails arising from the emission occurring in flight during the stopping process of the  $^{66}\text{Ni}$  reaction product inside the target material. This happens when a state is fed directly and its lifetime is of the order of 1 to 2 ps.

The transitions to the first  $2^+$  state (at 1425.1 keV) from the  $0_2^+$  and  $0_3^+$  excited states are clearly visible in Fig. 2(b), with energies of 1018 and 1246 keV, respectively. A weaker 1546-keV line, depopulating the  $3^+$  state at 2971.0 keV, is also seen. It was verified that both 1018- and 1246-keV lines do not show any broadening, i.e., lifetimes longer than 2 ps are expected for the  $0_2^+$  and  $0_3^+$  states. In contrast, the 1546-keV peak (shown in the inset), is more complex: besides the broadening, which was used to extract a lifetime of 1.4(2) ps for the  $3^+$  state at 2971.0 keV (with the Doppler shift attenuation method [38]), a weak satellite line is observed on the right-hand side shoulder. We hypothesized that this satellite line, at approximate energy of 1549 keV, may be a transition from the  $0_4^+$  state of  $^{66}\text{Ni}$  to the first excited  $2^+$  state, which would then place this  $0^+$  excitation at 2974 keV. Our hypothesis was based on the fact that a  $0_4^+$  state located at 2965(10) keV in the low energy resolution ( $t, p$ ) reaction study of Ref. [33], after recalibrating the ( $t, p$ ) energy spectrum (using the precise transition energies of Ref. [34]), turned out to correspond to a level deexcited by the 1549-keV  $\gamma$  ray. This interpretation is also supported by the intensity ratios between the  $\gamma$  decay from the excited  $0^+$  states, i.e.,  $I(1018)/I(1246) = 0.7$  and  $I(1549)/I(1246) = 0.05$ , which are of the same order as the ones established in the ( $t, p$ ) reaction (0.6 and 0.15), respectively.

As the next step, we performed a lifetime measurement of the three  $0^+$  excited states decaying via the observed 1018-, 1246-, and 1549-keV transitions, by applying



the plunger technique. We used the same reaction,  $^{18}\text{O}(39\text{ MeV}) + ^{64}\text{Ni}$ , but a thinner  $1\text{ mg/cm}^2$  target, in order to assure that all  $^{66}\text{Ni}$  recoils exit the target material. The average velocity of the recoils was  $v/c \approx 2.2\%$ , corresponding to a time-of-flight of  $\approx 155\text{ ps}$  over a  $1\text{ mm}$  distance. For each  $\gamma$ -ray transition, the fraction of  $\gamma$  decay occurring in a Ta stopper ( $5\text{ mg/cm}^2$  thick), placed at 12 distances from the target (i.e., 10, 20, 25, 40, 50, 60, 100, 200, 500, 1000, 2000, and  $3000\ \mu\text{m}$ ) was measured.

Figures 3(a) and 3(b) show partial  $\gamma$ -ray spectra gated on the  $1425\text{-keV } 2^+ \rightarrow 0^+$  transition of  $^{66}\text{Ni}$ , which were measured at short and long target-to-stopper distances, respectively. The spectrum in panel (a) is the sum of all spectra taken at stopper distances  $10\text{--}100\ \mu\text{m}$ , which can be translated in the time-of-flight range  $1.5\text{--}15\text{ ps}$ . Two well pronounced, sharp peaks correspond to the decay in the stopper of the  $0_2^+$  and  $0_3^+$  states, via the  $1018\text{-}$  and  $1246\text{-keV } \gamma$  rays, respectively. No in-flight components are visible due to the large spreading of the products velocity vectors. In turn, Fig 3(b) displays a summed spectrum for the distances  $500\text{--}3000\ \mu\text{m}$  - it corresponds to the time-of-flight range  $75\text{--}450\text{ ps}$ . Here, only one pronounced line at  $1246\text{ keV}$  is seen.

It was clear then that the  $0_2^+$  state would have a lifetime of the order of  $10\text{ ps}$  while the  $0_3^+$  excitation would decay with

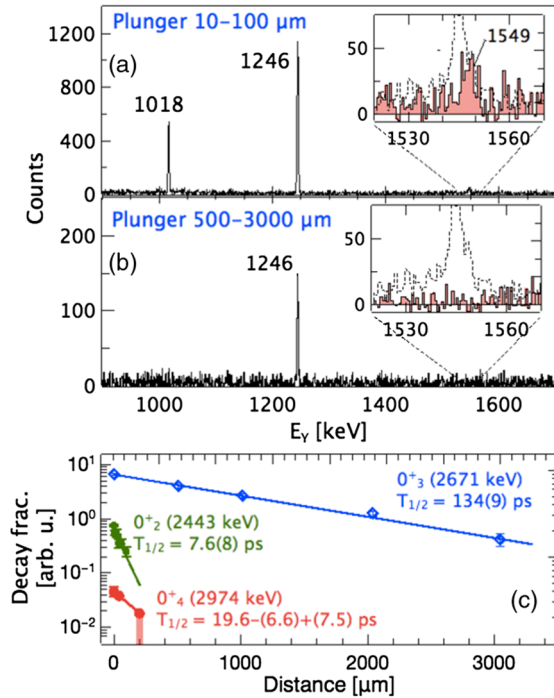


FIG. 3. (a)–(b) Portions of  $\gamma$  spectra obtained with the plunger setup, in coincidence with the  $1425\text{-keV}$  transition [(a) sum over the short, (b) sum over the long distances]. The zoom around the  $1546\text{-keV}$  transition is shown in the insets. The dashed histograms display the corresponding thick target spectrum, for comparison. (c) Decay curves of the three excited  $0^+$  states of  $^{66}\text{Ni}$ , as a function of the target-to-stopper distance.

a lifetime longer than  $100\text{ ps}$ . The case of the  $0_4^+$  state, deexciting via a  $1549\text{-keV } \gamma$  ray, required special attention. The insets in Figs. 3(a) and 3(b) show the portion of the corresponding spectra around the energy of  $1549\text{ keV}$ . While in the thick-target spectrum [inset of Fig 2(b)] the peak around  $1546\text{ keV}$  is composed of the  $1546\text{-keV } 3^+ \rightarrow 2^+$  line and the satellite transition at  $1549\text{ keV}$ , as discussed earlier, in the plunger spectrum, corresponding to measurements at short distances [inset of Fig. 3(a)], only the  $1549\text{-keV } \gamma$  ray is seen. This observation is in line with both the previously established  $1.4\text{ ps}$  lifetime of the  $3^+$  state which deexcites via the  $1546\text{-keV } \gamma$  ray and the existence of the  $1549\text{-keV } 0_4^+ \rightarrow 2_1^+$  transition, which exhibits a lifetime longer than a few picoseconds. The nonobservation of the  $1549\text{-keV}$  line in the spectrum associated with larger plunger distances [inset in Fig. 3(b)] narrows the upper limit of the  $0_4^+$  state lifetime value to a few tens of picoseconds.

In order to extract precise values of the lifetime for the three  $0^+$  excited states, we developed an analysis procedure based on the Monte Carlo simulations of the reaction, energy loss in the target, plunger-target geometry, and  $\gamma$  emission in the plunger measurement. The initial velocity vector distribution of  $^{66}\text{Ni}$  products, after the  $2n$ -transfer reaction, was calculated using the semiclassical GRAZING model [39] - the average value of the velocity, with respect to  $c$ , perpendicular to the plunger was  $2.19\%$  with  $\sigma = 0.31\%$ .

The fraction of  $\gamma$ -ray decays in the stopper could then be simulated and a minimization procedure, with respect to the lifetime, was applied to the corresponding experimental data, at the considered distances. The lifetime uncertainty was determined by a Monte Carlo error estimate, taking into account the experimental errors.

The experimental values for the decay fraction of the  $1246\text{-keV}$  line, deexciting the  $0_3^+$  state, were obtained from the intensities of the stopped components (observed in coincidence with the  $2^+ \rightarrow 0^+$   $1425\text{-keV}$  transition, at each plunger distance), normalized to the  $147\text{-keV}$  line from the  $78.7\text{ ns}$  isomeric decay of  $^{79}\text{Kr}$ , produced in the fusion channel. The results are shown in Fig. 3(c), together with the decay curve corresponding to the half-life  $T_{1/2} = 134 \pm 9\text{ ps}$ , obtained from the minimization procedure described above.

In the case of the  $1018\text{-keV}$  line, deexciting the  $0_2^+$  state, the experimental values of the decay fractions were obtained by using for normalization the long-lived  $1246\text{-keV}$  transition mentioned above (correcting for its decay). The fitting procedure yielded the half-life value  $T_{1/2} = 7.6 \pm 0.8\text{ ps}$ , as shown in Fig. 3(c). For the  $1549\text{-keV } \gamma$  ray, depopulating the  $0_4^+$  state, a dedicated procedure was applied, owing to its very low intensity. Three experimental points were used: (i) the decay intensity of the  $1549\text{-keV } \gamma$  ray extracted from the thick target measurement, (ii) the decay fraction obtained by summing the plunger measurements between  $10$  and

100  $\mu\text{m}$ , and (iii) an upper limit for the decay fraction at 200  $\mu\text{m}$  distance. For each point, again the 1246-keV transition was used for normalization. Here, the minimization procedure was based on the experimental weight of the individual measurements between 10 and 100  $\mu\text{m}$  (corresponding to an effective distance of 40  $\mu\text{m}$ ). The value  $T_{1/2} = 19.6 - (6.6) + (7.5)$  ps was obtained, and the result is shown in Fig. 3(c). To estimate  $B(E2)$  reduced probabilities for the  $E2$  transitions deexciting the  $0^+$  states, possible  $E0$  branching into the  $0_{g.s.}^+$  should be considered. We have calculated upper limits for the squared dimensionless monopole transition strengths  $\rho^2(E0)$  within the simple two-level model of Ref. [40], considering the shapes predicted by the MCSM discussed above, and assuming maximum mixing. We obtained  $\rho^2(E0) \leq 0.018$  and  $\leq 0.09$  for the oblate and prolate configurations, respectively, leading to  $E0$  branches out of the  $0_2^+$  and  $0_4^+$  states  $\leq 0.1\%$  and  $\leq 3\%$ , respectively [41]. For the spherical  $0_3^+$  state the  $E0$  branch is expected to be negligible. Such low values of  $E0$  do not influence significantly the partial lifetimes for  $E2$  decay from the excited  $0^+$  states - their effect is well within the experimental uncertainty. Therefore, we adopt the  $B(E2)$  values of  $4.3 \pm 0.5$ ,  $0.09 \pm 0.01$ , and  $0.21 \pm 0.07$  W.u., for the  $0_2^+$ ,  $0_3^+$ , and  $0_4^+$  states, respectively. It is remarkable to note that both  $E2$  transitions from the  $0_3^+$  and  $0_4^+$  states are significantly retarded.

The MCSM calculations, discussed above, perfectly reproduce the  $0_2^+$  oblate state decay probability, while the calculated  $B(E2)$  values for transitions deexciting the spherical  $0_3^+$  and prolate  $0_4^+$  states are smaller than the experimental ones (i.e., 0.01 and 0.006 W.u., respectively). We remark that extremely small calculated  $B(E2)$  values ( $\ll 0.1$  W.u.) may be related to the omission of tiny components of the wave function, which would be picked up in a larger calculation.

In summary, we have measured lifetimes for all three  $0^+$  excited states in  $^{66}\text{Ni}$  by employing a two-neutron transfer reaction below the Coulomb barrier and the plunger technique. We found a substantial hindrance for the  $E2$  decay from the second and third excited  $0^+$  states. The MCSM calculations account well for the presence of all three excited  $0^+$  states and provide a good description of their  $E2$  decay probabilities. Of special interest is the hindrance measured for the  $E2$  transitions originating from the  $0_3^+$  spherical and  $0_4^+$  prolate state. While the retarded  $E2$  decay from the  $0_3^+$  state is due to cancellation effects among  $E2$  matrix elements, the retarded  $E2$  decay from the  $0_4^+$  state arises from a sizable potential barrier between the prolate (secondary) and spherical ground state minima [18]. This result makes the  $^{66}\text{Ni}$  nucleus a unique example of a nuclear system, apart from the actinides, in which a shape-isomerlike structure exists.

This work was supported by the Italian Istituto Nazionale di Fisica Nucleare, by the Polish National

Science Centre under Contracts No. 2014/14/M/ST2/00738 and No. 2013/08/M/ST2/00257, and by the Interuniversity Attraction Poles Programme (IAP) via the Belgian Science Policy Office (BriX network P7/12). It was supported by the Grants No. PN-II-RU-TE-2014-4-2003 and No. PNIII-IFA-CERN-RO-03-ISOLDE. It was also partially supported by Grants-in-Aid for Scientific Research (23244049), by HPCI Strategic Program (hp150224), by MEXT and JICFuS, by Priority Issue (Elucidation of the fundamental laws and evolution of the universe) to be Tackled by Using Post “K” Computer (hp160211), and by CNS-RIKEN joint project for large-scale nuclear structure calculations.

\*Corresponding author:  
silvia.leoni@mi.infn.it

- [1] C. M. Dobson, A. Šali, and M. Karplus, *Angew. Chem. Int. Ed.* **37**, 868 (1998).
- [2] S. Åberg, H. Flocard, and W. Nazarewicz, *Annu. Rev. Nucl. Part. Sci.* **40**, 439 (1990).
- [3] A. N. Andreyev *et al.*, *Nature (London)* **405**, 430 (2000).
- [4] E. Bouchez *et al.*, *Phys. Rev. Lett.* **90**, 082502 (2003).
- [5] J. L. Wood, K. Heyde, W. Nazarewicz, M. Huyse, and P. van Duppen, *Phys. Rep.* **215**, 101 (1992).
- [6] P. Van Duppen, E. Coenen, K. Deneffe, M. Huyse, K. Heyde, and P. Van Isacker, *Phys. Rev. Lett.* **52**, 1974 (1984).
- [7] P. Walker and J. Dracoulis, *Nature (London)* **399**, 35 (1999).
- [8] S. M. Polikanov, *Sov. Phys. Usp.* **15**, 486 (1973).
- [9] J. Kantele, W. Stoffl, L. E. Ussery, D. J. Decman, E. A. Henry, R. W. Hoff, L. G. Mann, and G. L. Struble, *Phys. Rev. Lett.* **51**, 91 (1983).
- [10] P. Butler, R. Daniel, A. D. Irving, T. P. Morrison, P. J. Nolan, and V. Metag, *J. Phys. G* **6**, 1165 (1980).
- [11] B. Singh, R. Zywina, and R. Firestone, *Nucl. Data Sheets* **97**, 241 (2002).
- [12] P. Bonche, S. J. Krieger, P. Quentin, M. S. Weiss, J. Meyer, M. Meyer, N. Redon, H. Flocard, and P.-H. Heenen, *Nucl. Phys. A* **500**, 308 (1989).
- [13] M. Girod, J. P. Delaroche, and J. F. Berger, *Phys. Rev. C* **38**, 1519(R) (1988).
- [14] M. Girod, J. P. Delaroche, D. Gogny, and J. F. Berger, *Phys. Rev. Lett.* **62**, 2452 (1989).
- [15] P. Möller, A. J. Sierk, R. Bengtsson, H. Sagawa, and T. Ichikawa, *Phys. Rev. Lett.* **103**, 212501 (2009).
- [16] P. Möller, A. J. Sierk, and A. Iwamoto, *Phys. Rev. Lett.* **92**, 072501 (2004).
- [17] Y. Tsunoda, T. Otsuka, N. Shimizu, M. Honma, and Y. Utsuno, *Phys. Rev. C* **89**, 031301(R) (2014).
- [18] T. Otsuka and Y. Tsunoda, *J. Phys. G* **43**, 024009 (2016).
- [19] S. Lenzi, F. Nowacki, A. Poves, and K. Sieja, *Phys. Rev. C* **82**, 054301 (2010).
- [20] T. Togashi, Y. Tsunoda, T. Otsuka, and N. Shimizu, *Phys. Rev. Lett.* **117**, 172502 (2016).
- [21] C. Kremer *et al.*, *Phys. Rev. Lett.* **117**, 172503 (2016).
- [22] F. Nowacki, A. Poves, E. Caurier, and B. Bounthong, *Phys. Rev. Lett.* **117**, 272501 (2016).

- 
- [23] T. Otsuka, M. Honma, T. Mizusaki, N. Shimizu, and Y. Utsuno, *Prog. Part. Nucl. Phys.* **47**, 319 (2001).
- [24] N. Shimizu, Y. Utsuno, T. Mizusaki, T. Otsuka, T. Abe, and M. Honma, *Phys. Rev. C* **82**, 061305(R) (2010).
- [25] N. Shimizu, T. Abe, Y. Tsunoda, Y. Utsuno, T. Yoshida, T. Mizusaki, M. Honma, and T. Otsuka, *Prog. Theor. Exp. Phys.* **2012**, 01A205 (2012).
- [26] N. Shimizu, Y. Utsuno, T. Mizusaki, M. Honma, Y. Tsunoda, and T. Otsuka, *Phys. Rev. C* **85**, 054301 (2012).
- [27] W.F. Mueller *et al.*, *Phys. Rev. C* **61**, 054308 (2000).
- [28] C. J. Chiara *et al.*, *Phys. Rev. C* **86**, 041304(R) (2012).
- [29] C. J. Prokop *et al.*, *Phys. Rev. C* **92**, 061302(R) (2015).
- [30] A. I. Morales *et al.*, *Phys. Lett. B* **765**, 328 (2017).
- [31] B. P. Crider *et al.*, *Phys. Lett. B* **763**, 108 (2016).
- [32] S. Suchyta *et al.*, *Phys. Rev. C* **89**, 021301(R) (2014).
- [33] W. Darcey, R. Chapman, and S. Hinds, *Nucl. Phys.* **A170**, 253 (1971).
- [34] R. Broda *et al.*, *Phys. Rev. C* **86**, 064312 (2012).
- [35] S. N. Liddick *et al.*, *Phys. Rev. C* **85**, 014328 (2012).
- [36] D. Pauwels, ARIS-2011 Conference (Leuven, Belgium) [iks32.fys.kuleuven.be/indico/event/0/page/20](https://iks32.fys.kuleuven.be/indico/event/0/page/20).
- [37] D. Bucurescu *et al.*, *Nucl. Instrum. Methods Phys. Res., Sect. A* **837**, 1 (2016).
- [38] P. J. Nolan and J. F. Sharpey-Schafer, *Rep. Prog. Phys.* **42**, 1 (1979).
- [39] A. Winther, *Nucl. Phys.* **A594**, 203 (1995).
- [40] J.L. Wood, E.F. Zganjar, C. De Coster, and K. Heyde, *Nucl. Phys.* **A651**, 323 (1999).
- [41] T. Kibédi, T.W. Burrows, M.B. Trzhaskovskaya, P.M. Davidson, and C.W. Nestor Jr., *Nucl. Instrum. Methods Phys. Res., Sect. A* **589**, 202 (2008).